

RESEARCH ARTICLE

Representation of the wintertime Arctic Oscillation in a multi-model ensemble

Gayoung Kim¹  | Joong-Bae Ahn² 

¹Climate Service and Research Division,
APEC Climate Center, Busan, South
Korea

²Department of Atmospheric Sciences,
Pusan National University, Busan, South
Korea

Correspondence

Joong-Bae Ahn, Department of
Atmospheric Sciences, Pusan National
University, Geumjeong-gu, Busan 46241,
South Korea.

Email: jbahn@pusan.ac.kr

Funding information

Cooperative Research Program for
Agriculture Science & Technology
Development, Rural Development
Administration, Republic of Korea, Grant/
Award Number: PJ01489102; APEC
Climate Center

Abstract

The Arctic Oscillation (AO) is a well-known mode that affects climate variability in the Northern Hemisphere. The equal-weighted multi-model ensemble (MME) of six state-of-the-art models from the Copernicus Climate Change Service (C3S) and Pusan National University (PNU) was analysed to understand the wintertime AO performance for the hindcast period December–February 1993/1994–2016/2017. The hindcasts were chosen with lead times of 1 and 4 months with respect to the initialization date (August and November, respectively). The spread of the AO prediction skills of the individual models was significant. In general, the MME demonstrates superior skill compared to the average of single-model skills in representing the AO pattern at lead times of 1 and 4 months. The AO-related vertical structure predicted by MME is similar to the observation, but the upper-level structure is relatively poor compared to the structure of the hindcasted lower- or mid-level atmosphere. Both observation and MME indicate that since the mid-1990s, the relationship between the AO and East Asian winter monsoon (EAWM) has been weak compared to the connection between the AO and El Niño–Southern Oscillation (ENSO). Simultaneously, the North Pacific centre of the AO moved eastward during the observational period. The MME showed an AO pattern similar to that observed. The eastward shift of the North Pacific centre of the AO may contribute to deepening the Aleutian low and its effect on the tight AO–ENSO relation demonstrated in observations and MME. Strong AO–ENSO relations and weak AO–EAWM connections are found in both observations and MME model. The observation and MME represent the wave activity flux from 60°N to the equator in the troposphere; consequently, the wave activity flux may contribute to the AO and ENSO connection in both observation and MME.

KEYWORDS

Aleutian low, Arctic Oscillation, El Niño–Southern Oscillation, multi-model ensemble

1 | INTRODUCTION

A recent study suggested that Arctic sea ice or Arctic climate variability can affect mid-latitude weather/climate (Cohen *et al.*, 2020). However, most seasonal prediction

models cannot capture such extreme events properly (Shin and Moon, 2018). Many studies regarding dynamical predictions have focused on tropical ocean variability, such as the El Niño–Southern Oscillation (ENSO), which can be forecasted several months ahead and directly

influences forecast skill through teleconnection with mid-latitude weather or climate (Palmer *et al.*, 2004; Jin *et al.*, 2008; Wang *et al.*, 2009; Doblas-Reyes *et al.*, 2013). Modelling studies have expanded their scope to improve forecast skills at mid-latitudes by improving the simulation of the Indian Ocean dipole (IOD) and the Madden-Julian Oscillation (MJO) on a subseasonal to interannual timescale (Palmer *et al.*, 2004; Doblas-Reyes *et al.*, 2013).

The Arctic Oscillation (AO) is one of the dominant modes of atmospheric circulation over the Northern Hemisphere (NH; Thompson and Wallace, 1998; 2000). It primarily features a large-scale “seesaw” pattern between the Arctic Basin and the NH mid-latitudes. These patterns can be a signature of the polar vortex strength variations. The AO is strongly related to surface air temperature fluctuations over the Eurasian continent (Thompson and Wallace, 1998; Wang *et al.*, 2005). The AO is linked to the East Asian winter monsoon (EAWM) through large-scale circulation, such as the East Asian jet stream, the Siberian high (SH), and stationary planetary waves (Gong *et al.*, 2001; Wu and Wang, 2002a; 2002b; Jeong and Ho, 2005; Park *et al.*, 2010).

Although the AO is connected with the East Asian winter climate, there are insufficient studies regarding the AO using operational seasonal prediction models. However, some efforts have been made to understand AO variability using climate change scenarios. Zuo *et al.* (2013) evaluated the temporal variability and spatial pattern of the AO simulated in a historical experiment of 26 coupled climate models participating in the Coupled Model Intercomparison Project Phase 5 (CMIP5). They reported that only a few models could reproduce the temporal variability and spatial structures in both horizontal and vertical directions. Lee *et al.* (2020) represented the characteristics of the wintertime AO and the North Atlantic Oscillation (NAO) and their impact on climate variability over the NH simulated by a historical dataset using the Energy Exascale Earth System Model version 1 (E3SM). The E3SM contributes to the Coupled Model Intercomparison Phase 6 (CMIP6). They suggested that the simulated AO and NAO modes have spatial structures similar to the observed features, but the vertical structures associated with the AO and the NAO in E3SM exhibit substantial biases in the lower stratosphere caused by the strength of the climatological stratospheric polar vortex and wave activity fluxes. Li *et al.* (2018) reported the relationship between the EAWM and the winter AO using historical simulations and future projections under Representative Concentration Pathway (RCP) 4.5 and 8.5 scenarios from 33 CMIP5 models. They reported that the observed evaluation of the EAWM–AO relationship could be reproduced well by coupled models. The link between the winter AO on the EAWM-related circulation and East

Asian winter temperatures was intensified by the propagation of stationary planetary waves.

Sun and Ahn (2015) showed the predictability of the wintertime AO using a coupled model named the Pusan National University coupled general circulation model (PNU CGCM) for a 30-year retrospective period. The performance of the model was more than satisfactory in terms of the spatial distribution and temporal variation of the AO impact on the NH winter climate. Kang *et al.* (2014) assessed the AO prediction skills of six state-of-the-art dynamical models using both deterministic and probabilistic methods. They reported that most dynamical models have consistently improved their skill scores for lead times of up to 2 months during the winter. In addition, they suggested some possibilities for skilfully predicting the AO and related climate anomalies on a seasonal timescale.

Motivated by previous studies, we investigate the prediction skill of models for the wintertime AO using the MME on a seasonal timescale. The data and methods are introduced in section 2. Section 3 describes the general performance of the wintertime AO using the MME and the recent AO–ENSO relationship. Conclusions and discussion are presented in section 4.

2 | DATA AND METHODS

2.1 | Data

The seasonal forecast data from six prediction systems were analysed, five from models from the C3S seasonal forecast and the PNU CGCM database (Table 1). All the models used in this study provided three-dimensional atmospheric data for the recent hindcast period. The C3S models used were from the European Center for Medium-range Weather Forecast (ECMWF), United Kingdom Met Office (UKMO), Météo-France, Deutscher Wetterdienst (DWD), and Euro-Mediterranean Centre on Climate Change (Centro Euro-Mediterraneo sui Cambiamenti Climatici, CMCC). The final of the six models, the PNU CGCM is utilized by the APEC Climate Center (APCC). The 1- and 4-month lead hindcasts for the boreal winter seasons (December–February [DJF]) initialized in November and August were evaluated.

ERA-Interim from the European Center for Medium-Range Weather Forecasts (ECMWF) (Dee *et al.*, 2009; 2011) and the NOAA Optimum Interpolation (OI) Sea Surface Temperature (SST) V2 (Reynolds *et al.*, 2007) were used as observational references. Sea-level pressure, sea surface temperature, three-dimensional temperature, zonal wind, and geopotential height were used for the common hindcast period during 1993–2016 (24 years). All datasets were interpolated into a grid with a resolution of 2.5° for both the longitude and latitude.

TABLE 1 Summary of models used in this study

Originating centre	Model name	Subset	Resolution (atmos.)	Hindcast ensemble size	cHindcast period
ECMWF	SEAS5	C3S	TCO319/L91	25	1981–2016
UK Met Office	GloSea5-GC2-LI	C3S	N216/L85	28	1993–2016
Météo-France	Météo-France System 7	C3S	TL359/L91	25	1993–2016
DWD	GCFS 2.0	C3S	T127/L95	30	1993–2017
CMCC	CMCC-SPS3	C3S	Approx. 0.5° lat-long/L46	40	1993–2016
PNU	PNU CGCM 2.0	APCC	T42/L18	35	1980–present

2.2 | Methods of analysis

The MME method used in this study is a grand ensemble mean that arithmetically averages all hindcasts, assuming that each ensemble member of each model is equally probable. Many operational centre (e.g., Development of a European Multimodel Ensemble System for Seasonal-To-Interannual Prediction [DEMETER], North American Multi-Model Ensemble [NMME]) use this method to combine models (Palmer *et al.*, 2004; Kirtman *et al.*, 2014). The AO index was calculated by projecting the first empirical orthogonal function (EOF) mode in the NH (20°–90°N), at a geopotential height of 500 hPa (Z500), for field anomalies onto the reanalysis and hindcast data. The AO pattern was obtained by a forecast of Z500 anomalies regressed onto the AO index for each model (Kang *et al.*, 2014). The Niño3.4 index is calculated by the average sea surface temperature anomaly in the region bounded by 5°S–5°N, 170°–120°W for the observation and hindcast data. The SH index is defined as the domain-averaged sea-level pressure at 40°–60°N and 70°–120°E (Gong *et al.*, 2001). The East Asian trough (EAT) index is calculated by the Z500 average in 25°–45°N and 110°–145°E. The EAT is closely associated with the EAWM and cold surge activity (Wang and He, 2012). The three-dimensional wave activity flux, which represents the propagation of quasi-stationary Rossby waves, was estimated using the methodology described by Takaya and Nakamura (2001). The wave activity flux was used to analyse the wave propagation in the mean flow associated with the AO.

3 | RESULTS

3.1 | General performance of wintertime AO

The AO is characterized by a zonally symmetric pattern with clear opposite-signed anomalies between the Arctic and mid-latitude oceans. A negative anomalous centre is

situated over the Arctic, and the two positive anomalous centres lie over the North Pacific and North Atlantic (e.g., Thompson and Wallace, 1998; Kang *et al.*, 2014; Kryzhov and Gorelits, 2015; Sun and Ahn, 2015). Figure 1a shows the AO pattern from the observations during DJF 1993/1994–2016/2017. This reveals a zonally symmetric pattern that is slightly different from the AO pattern observed in Thompson and Wallace (1998, 2000). The North Pacific centre leans to the east and the North Atlantic centre extends zonally from the eastern part of North America to East Asia. The 1-month lead MME shows the opposite-orientated anomalies between the Arctic and mid-latitudes, with a pattern correlation coefficient of 0.68. However, the negative anomaly over the Arctic is underestimated, and a positive anomaly across the Eurasian continent is absent (Figure 1b). This may be because most individual models fail to capture positive anomalies in the Eurasian continent (Figure 1c–h).

The individual models represent the anomaly correlation coefficient (ACC) within the range of 0.22–0.66 for the AO indices and pattern correlation coefficient (PCC) within the range of 0.35–0.74 for the AO patterns for 1- and 4-month leads (Figure 2), respectively. Although the three models performed better than the MME for the 1-month lead, there was a large difference in performance between the models. Overall, the mean of the single-model skills is less than that of the MME, indicating that the general AO performance of the individual model is inferior to that of the MME. For the 4-month lead, the skills of individual models except for the ECMWF and MME decreased compared to the 1-month lead. This suggests that the predictability of AO can be guaranteed up to a 4-month lead using MME. Nevertheless, MME still represents superior skill compared to the mean of single-model skills (Kim *et al.*, 2016; 2021).

Figure 3 shows the zonal mean vertical structures of the geopotential height, zonal wind, and temperature anomalies regressed onto the wintertime AO indices for observation, the 1-month lead MME, and the 4-month lead MME. The observed geopotential height represents a meridional tripolar structure, and the zonal winds show

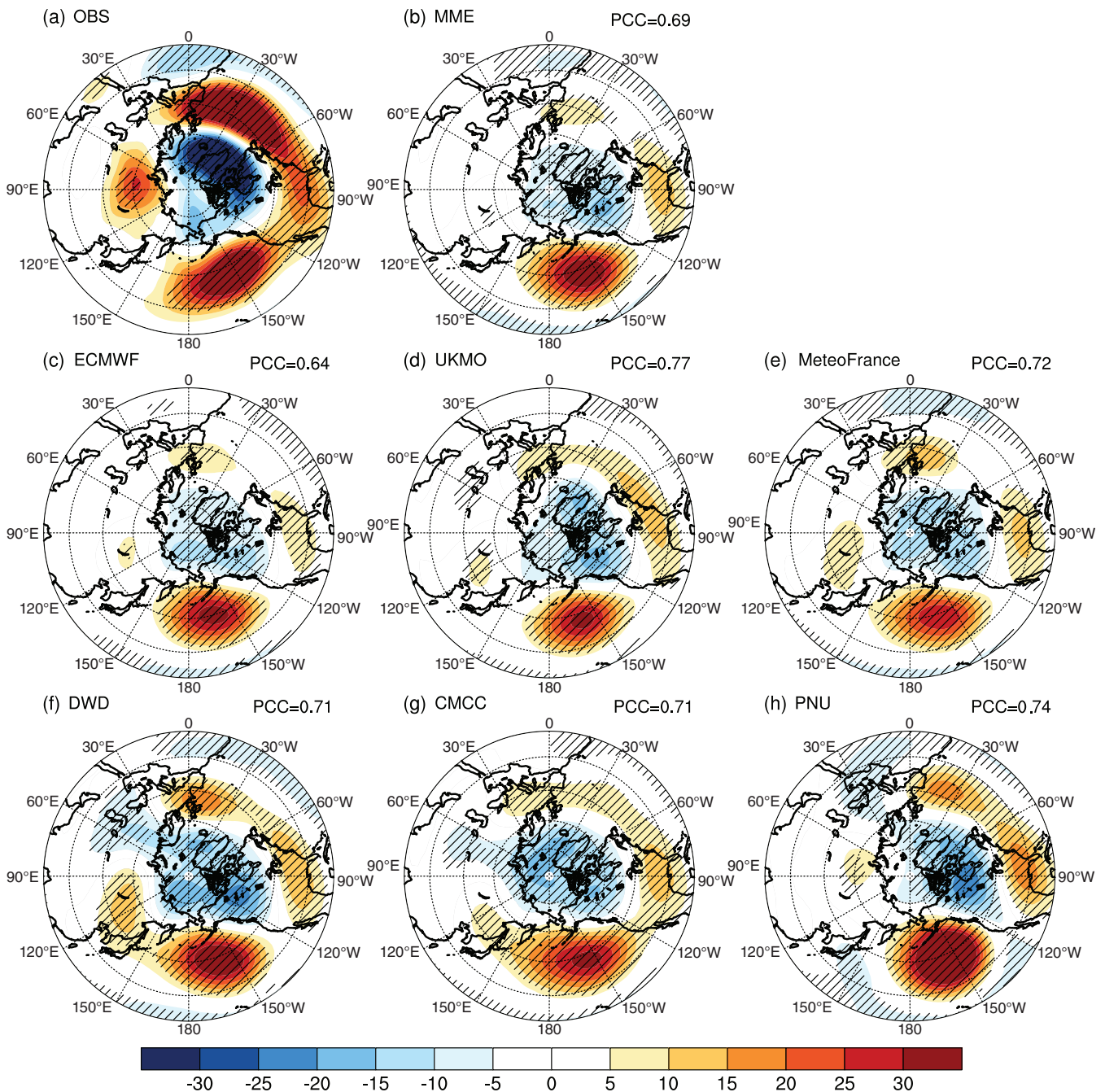


FIGURE 1 AO patterns of (a) observation, (b) MME and (c–h) individual models for 1-month lead over the domain poleward of 20°N during the period DJF 1993/1994–2016/2017. The hatched line indicates the statistical significance at the 95% confidence level using a 2-tailed Student's t test. The numbers in the top right corner of MME and individual models show the pattern correlation coefficient with the observation [Colour figure can be viewed at wileyonlinelibrary.com]

a meridional dipole structure from the surface to the lower stratosphere. The anomalies reverse near 60°N for geopotential height and 40°N for zonal winds. For zonal wind, the westerly anomalies over the polar region tilt poleward with height. The negative temperature anomaly over the polar cap from 500 to 10 hPa was dominant (Thompson and Wallace, 2000; Zuo *et al.*, 2013; Lee *et al.*, 2020). Although the magnitudes of all variables for the MME are

smaller than those of the observation, the MME can reproduce the AO-related vertical structures for a 1-month lead relatively accurately. The MME also captures the negative centre of action for a geopotential height anomaly and poleward-tilted westerly anomalies at high latitudes. However, there is a limit to reproducing the anomaly pattern of the geopotential height in the low- and mid-latitudes of the stratosphere by MME because most individual models

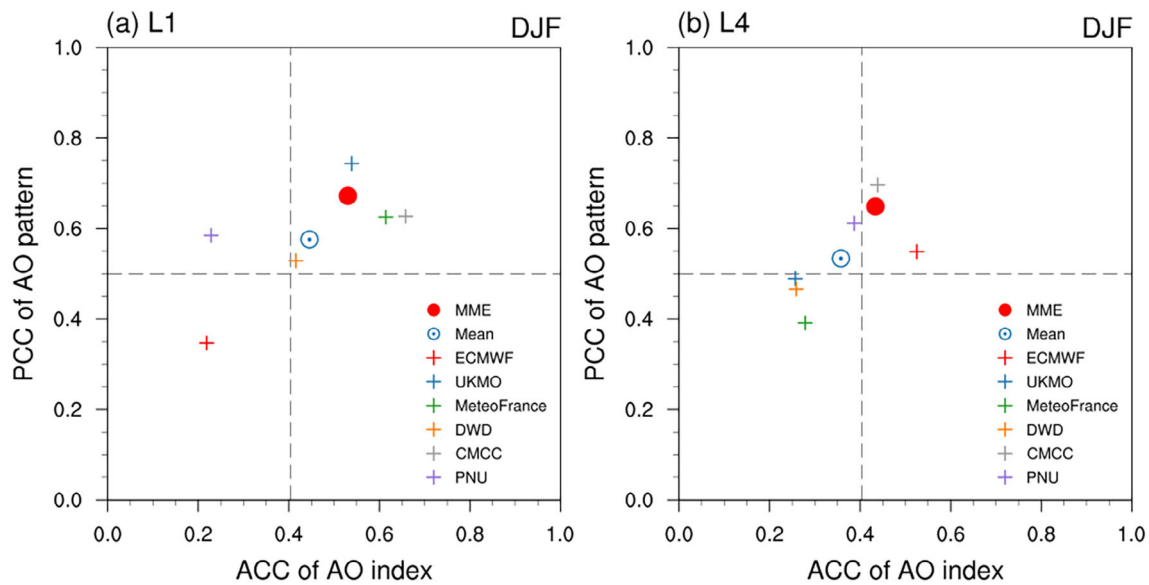


FIGURE 2 Scatter plot of anomaly correlation coefficient of AO indices and pattern correlation coefficient of AO patterns between observation and MME (red closed circle), individual models (crosses) and mean of single-model skills (mean; blue open circle with dot). The vertical grey dashed line indicates the statistical significance at the 95% confidence level using the 2-tailed Student's *t* test [Colour figure can be viewed at wileyonlinelibrary.com]

cannot capture the anomaly pattern (Figure S1, Supporting Information). For the 4-month lead, the magnitudes of all variables are much smaller than those of the 1-month lead of the MME and those of the individual models (Figures S1–S6). Figure 3d–f show that the observed maximum westerly anomaly over the tropical region is located at 30 hPa for the 1-month lead, but at 10 hPa for the 4-month lead MME.

Figure 4a shows the pattern correlation of the meridional AO structure between the observation and MME at each pressure level for each lead month. This figure demonstrates the excellent MME prediction of the zonal mean vertical structure associated with the AO. The MME reproduces the geopotential height relatively accurately for the 1- and 4-month leads with a statistical confidence level of 95%. The most notable feature of the 4-month lead geopotential height is that the pattern correlation decreases gradually with height but increases again above heights of 30 hPa. The pattern correlation of the MME decreases most significantly with the lead time in the lower stratosphere (100–50 hPa). In Figure S7, three models, ECMWF, UKMO, and DWD, exhibit a meridional structure with a height similar to the observations. This indicates that the pattern correlation with the 1-month lead is superior to that of the 4-month lead. Two of the models, Météo-France and CMCC, show pattern correlations greater than 0.80 for 1- and 4-month leads at all pressure levels. PNU has a better pattern correlation with the geopotential height from the surface to 30 hPa at the 4-month lead than that of the 1-month lead.

In the case of meridional-pattern of AO for the zonal wind, the MME performances for the 1- and 4-month lead were not significantly different but decreased rapidly at 10 hPa (Figure 4b). In Figure S8, the ECMWF and Météo-France represent a similar meridional structure with the height for the 1- and 4-month leads from the surface to the height of 30 hPa. The pattern correlations of the other models decrease sharply at heights above 50 hPa for both the 1- and 4-month leads.

In Figure 4c, the meridional-pattern correlation for temperature between the observation and the 4-month lead fluctuates more than the other variables. The pattern correlation of the MME is low in the lower troposphere, but it increases rapidly at a height of 500 hPa for both lead times. The pattern correlation for the 1-month lead remains relatively steady but is unstable for the 4-month lead MME. The maximum difference in the correlation for temperature is 0.89 at a height of 100 hPa.

Although there are differences depending on the variables, the overall 1-month forecast AO-pattern representation was superior to the 4-month performance. The performance of the geopotential and zonal wind showed that it is quite predictable even in the 4-month lead predictions using the MME. The CMCC showed a larger pattern correlation coefficient than other models for both 1 and 4 months, and it was relatively constant compared to the other models between the heights of 400 and 30 hPa (Figure S9). According to Portal *et al.* (2021), the CMCC performs comparably to a model with a far more resolved stratosphere.

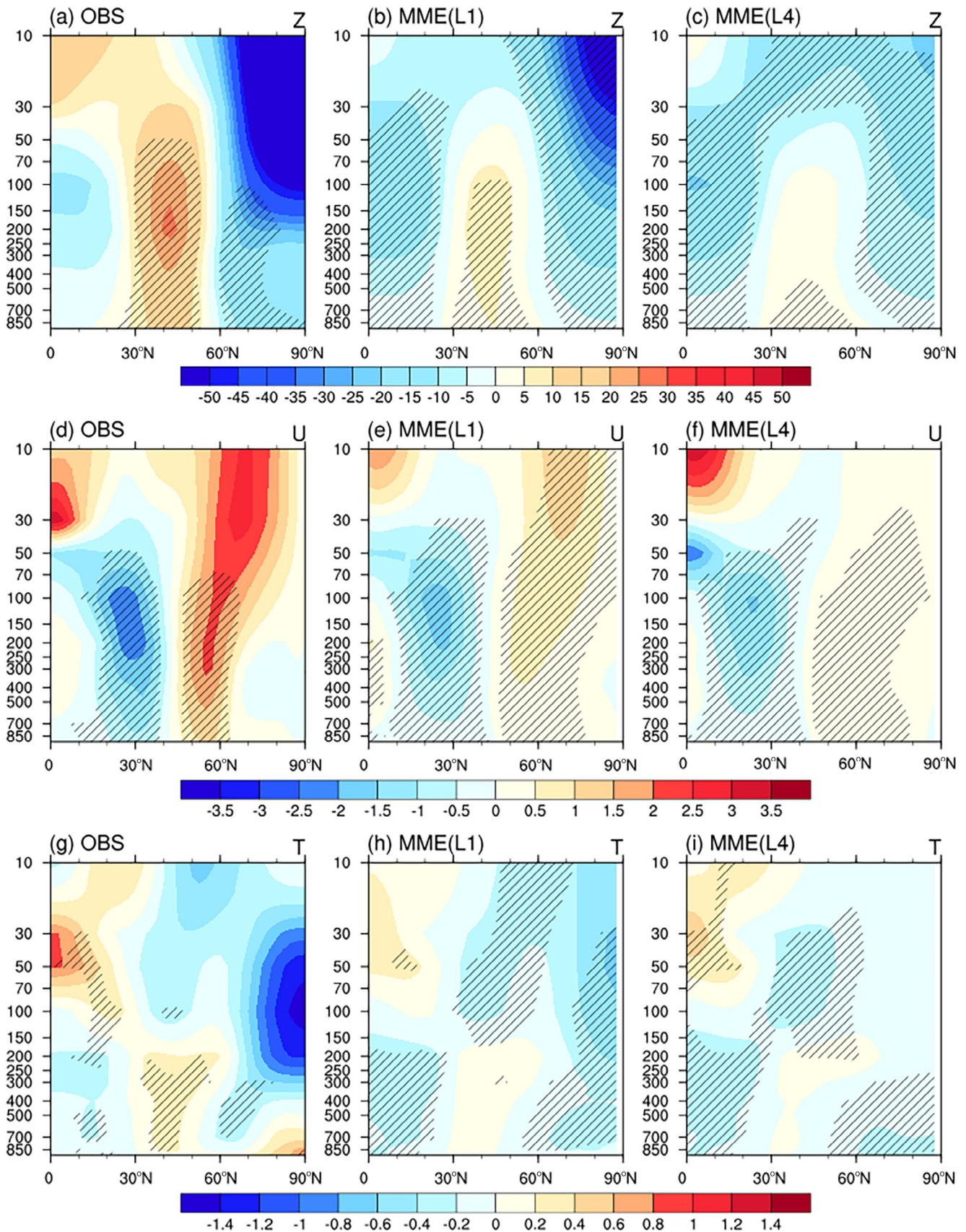


FIGURE 3 Vertical structure of the zonal mean (top) geopotential height (unit: m), (middle) zonal wind (unit: $\text{m}\cdot\text{s}^{-1}$), and (bottom) temperature (unit: K) regressed on the (a, d, g) observed AO index and (b, e, h) 1-month lead and (c, f, i) 4-month lead MME AO index. The hatched line indicates statistical significance at the 95% confidence level using the 2-tailed Student's *t* test [Colour figure can be viewed at wileyonlinelibrary.com]

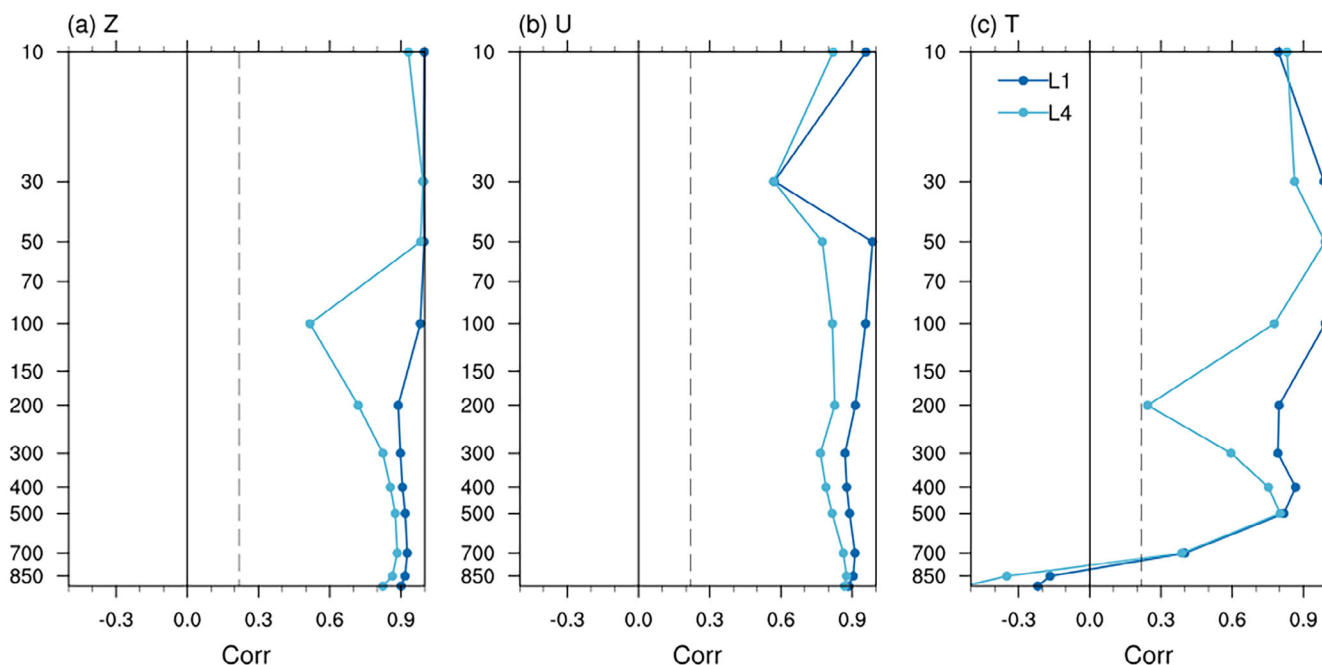


FIGURE 4 Correlation as a function of the pressure level between observation and MME for 1- and 4-month leads for zonal mean (a) geopotential height, (b) zonal wind, and (c) temperature, respectively. The grey dashed lines indicate that the estimated score is significant at a 95% confidence level using the 2-tailed Student's *t* test [Colour figure can be viewed at wileyonlinelibrary.com]

3.2 | AO–EAWM and AO–ENSO relationships

The AO is strongly connected to the SH and the EAT, which, in turn, affects the EAWM (Thompson and Wallace, 2000; Gong *et al.*, 2001; Wu and Wang, 2002a; Gong and Wang, 2003). Furthermore, the relationship between the AO and ENSO has been studied recently (Chen *et al.*, 2014; Li *et al.*, 2014; Chen *et al.*, 2018). The 11-year moving correlation coefficient between the AO index and SH, EAT, and negative Niño3.4 indices of observation, as well as MME for 1- and 4-month leads during DJF 1993/1994–2016/2017, are illustrated in Figure 5. SH and EAT were chosen as indices that represent the EAWM. During DJF 1993/1994–2016/2017, the observed AO–SH relationship was weak and the correlation between the AO and the EAT negative. However, the AO–ENSO relationship was more significant than that of the EAWM correlation. These features are inconsistent with those of previous studies (e.g., Gong *et al.*, 2001; Wu and Wang, 2002a; 2002b; Park *et al.*, 2010; Jeong *et al.*, 2017). Although the MME highlighted that since the mid-1990s, the AO–EAWM relationship is weaker than that of AO–ENSO, the correlation with AO–ENSO is much stronger for both 1- and 4-month leads than that of the observation. Furthermore, the AO–EAT correlation for the 4-month lead contrasts with that of the observation.

Figure 6a shows the regressed field of the sea-level pressure on the observed negative AO index. The negative AO phase is associated with a large-scale seesaw between the positive Arctic and negative mid-latitude sea level pressure. Negative sea-level pressure is located in the North Pacific and North Atlantic, and the centre of the North Pacific indicates deep Aleutian low pressure. East Asia is strongly influenced to the EAWM during winter, as represented by the robust SH over the Asian continent and the strong Aleutian low to its east (Chen *et al.*, 2000; Shin and Moon, 2018; Kim *et al.*, 2019). However, during DJF 1993/1994–2016/2017, the positive SH phase corresponded to positive sea-level pressure in the Siberian region only. The regression in Figure 6d does not show deepening of the Aleutian low. The ENSO-related sea-level pressure (Figure 6g) indicates a strong Aleutian low, similar to the regressed field on the negative AO index. For the MME, the negative AO index corresponds to positive Arctic and negative mid-latitude sea-level pressure, but the magnitude of positive sea-level pressure in the Arctic is weaker than that observed and disappears as the lead month increases. In contrast, negative sea-level pressure, which is related to the Aleutian low, was maintained with the 4-month lead (Figure 6b,c). The regressed pattern on the positive SH in the MME overestimates the east–west pressure gradient over the Pacific (Figure 6e,f). Although the magnitude was weaker over time, the regressed MME field on the positive ENSO

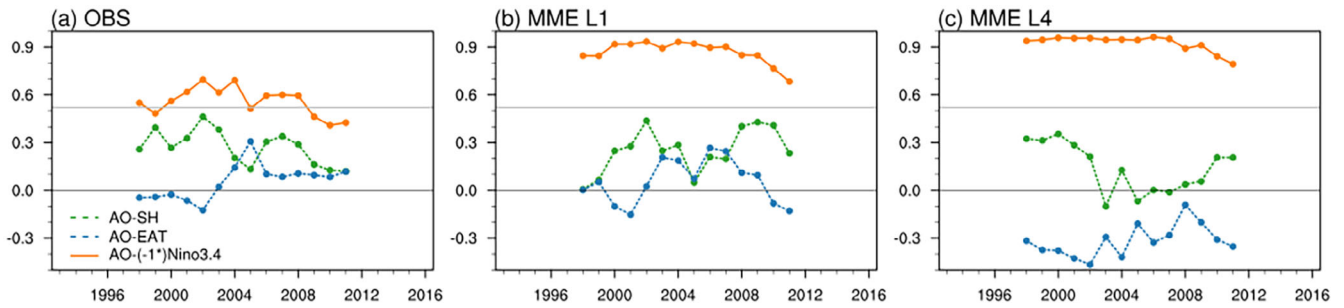


FIGURE 5 The 11-year moving correlation coefficient between AO and SH (green dashed line), AO and EAT (blue dashed line), and AO and negative Niño3.4 (Niño3.4, orange solid line) for (a) observation and MME for (b) 1-month and (c) 4-month leads during the period DJF 1993/1994–2016/2017. The grey solid lines indicate that the estimated score is significant at 95% confidence level using the 2-tailed Student's *t* test [Colour figure can be viewed at wileyonlinelibrary.com]

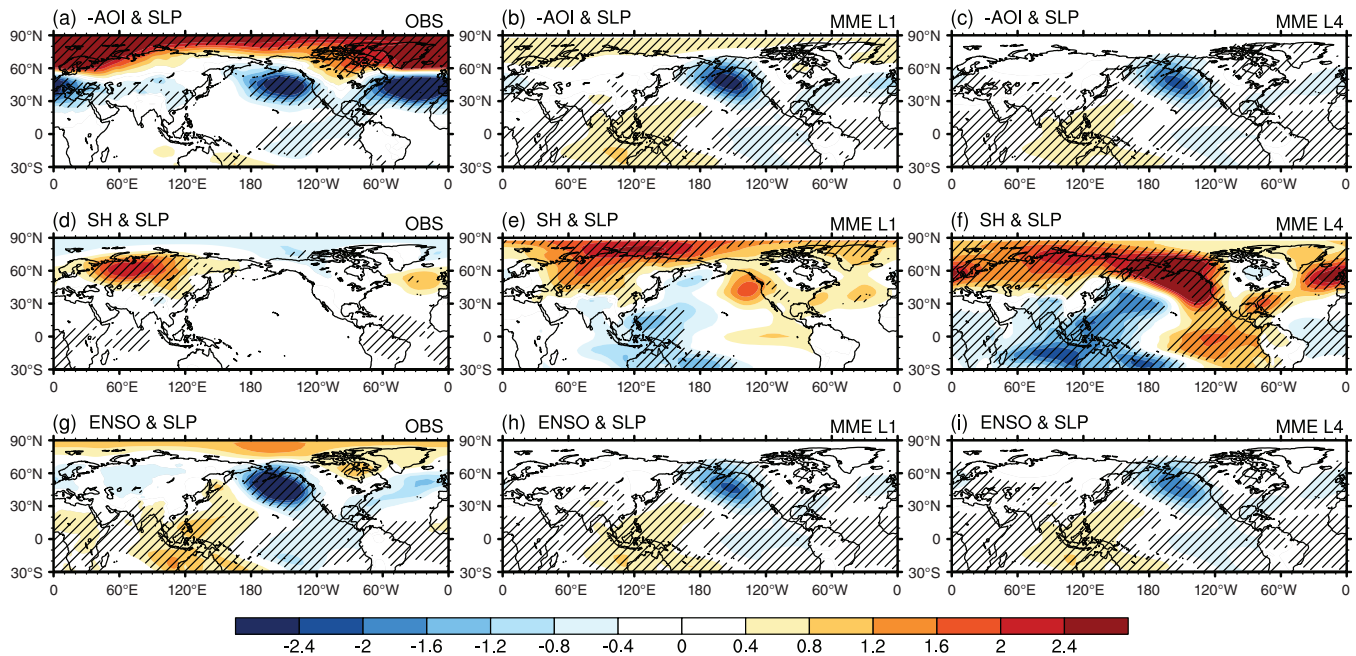


FIGURE 6 Sea-level pressure (unit: hPa) regressed on the (a, d, g) observation and (b, e, h) MME for 1-month and (c, f, i) 4-month leads (top) negative AO, (middle) positive SH, and (bottom) Niño3.4 indices for the DJF 1993/1994–2016/2017. The hatched line indicates statistical significance at the 95% confidence level using the 2-tailed Student's *t* test [Colour figure can be viewed at wileyonlinelibrary.com]

reproduced the observed fields, which showed a deepening Aleutian low (Figure 6h,i).

The observed low-level wind associated with the negative phase of the AO is characterized by cyclonic circulation in the North Pacific and is closely related to the Aleutian low. This low-level wind field in the North Pacific is more similar to the ENSO than the SH. The ENSO-like sea surface temperature pattern corresponding to the negative AO index is more similar to the ENSO than to the SH (Figure 7a,d,g). Furthermore, in the MME from 1- to 4-month leads, both the low-level wind and sea surface temperature associated with a negative AO index resemble the ENSO-related pattern similar to that observed. In contrast, the SH-related MME fields

MME for low-level wind and sea surface temperature are opposite to those of the negative AO phase (Figure 7b–d, e,f,h,i), as reproduced in most models except for the CMCC (Figure S10).

The enhancement of the Aleutian low coincides with both the negative AO- and ENSO-related Z500 fields. The negative AO further generates a strong trough in the Siberian region. In contrast, the Z500 field associated with SH indicated a strengthening of the EAT (Figure 8a, d,g). The MME reproduces negative AO- and ENSO-related geopotential fields at a height of 500 hPa with relative accuracy until the 4-month lead, which is characterized by the deepening of the Aleutian low (Figure 8b,c,h, i). In contrast, the MME represents a strong EAT and

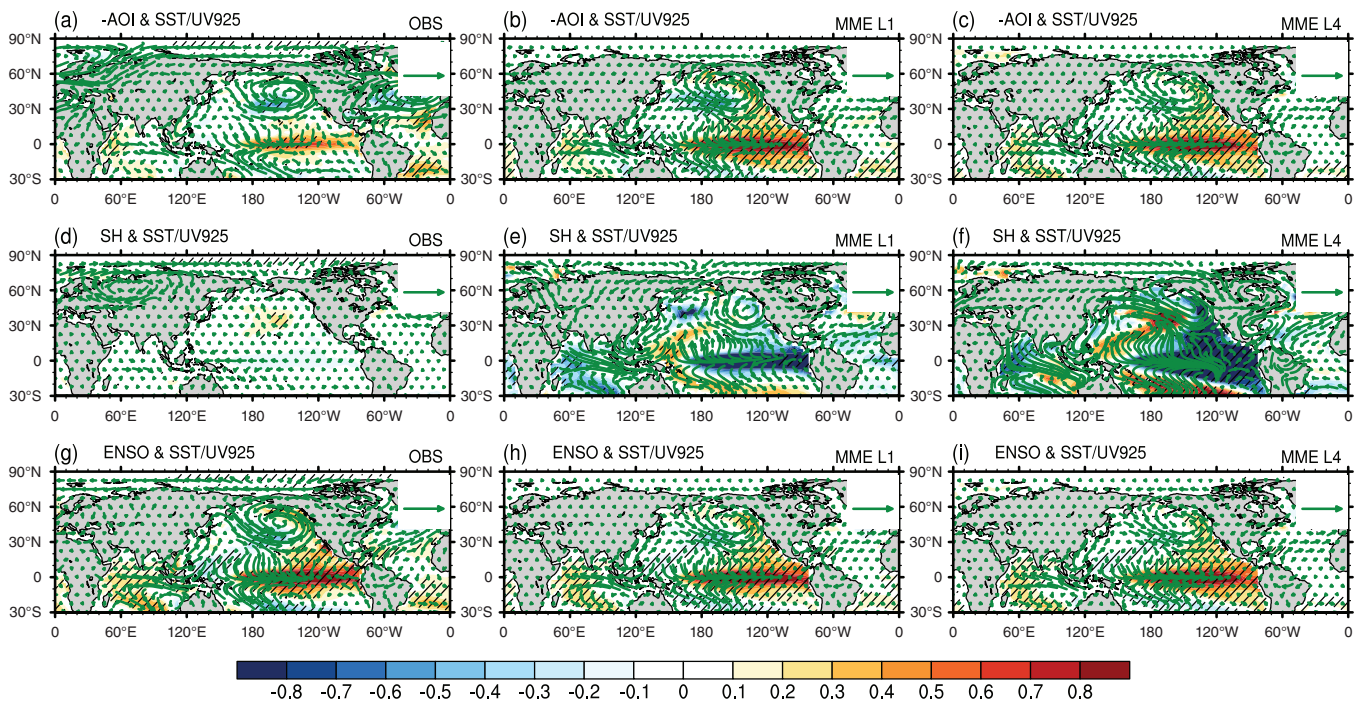


FIGURE 7 Same as Figure 6 but for sea surface temperature (unit: $^{\circ}\text{C}$) and 925 hPa wind vector (unit: $\text{m}\cdot\text{s}^{-1}$) [Colour figure can be viewed at wileyonlinelibrary.com]

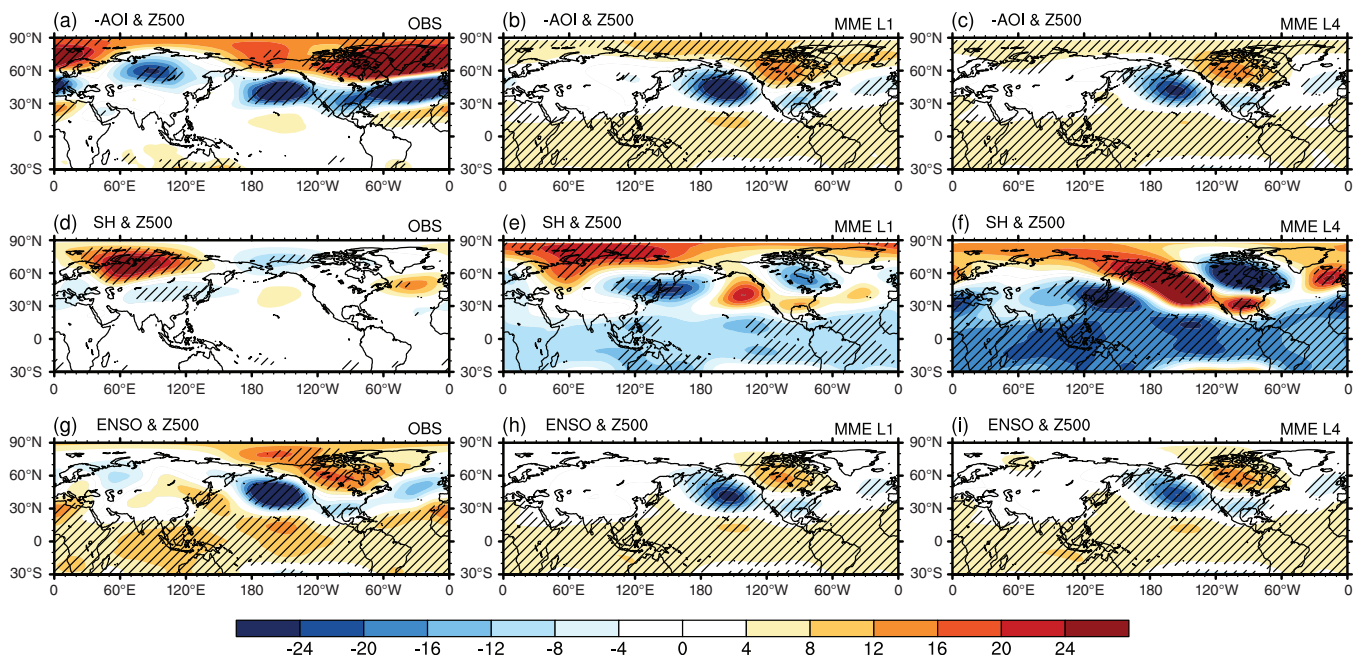


FIGURE 8 Same as Figure 6 but for Z500 (unit: m) [Colour figure can be viewed at wileyonlinelibrary.com]

weak Aleutian low associated with SH compared to that of the observation (Figure 8e,f).

As shown in Figure 7a–c, the AO and ENSO are strongly **connected** to the Aleutian low. According to Li *et al.* (2014), the strengthened link between the negative AO and Aleutian Low may help establish a closer relationship between the negative AO and ENSO. Figure 9

characterizes the vertical structure of the composite wave activity flux differences and that of the stream function in both the observations and MME to determine the mechanism by which waves propagate via negative AO near the Aleutian low (Figure 9). The wave activity flux and stream function were zonally averaged over the North Pacific (160°E – 120°W). A positive (negative) AO is

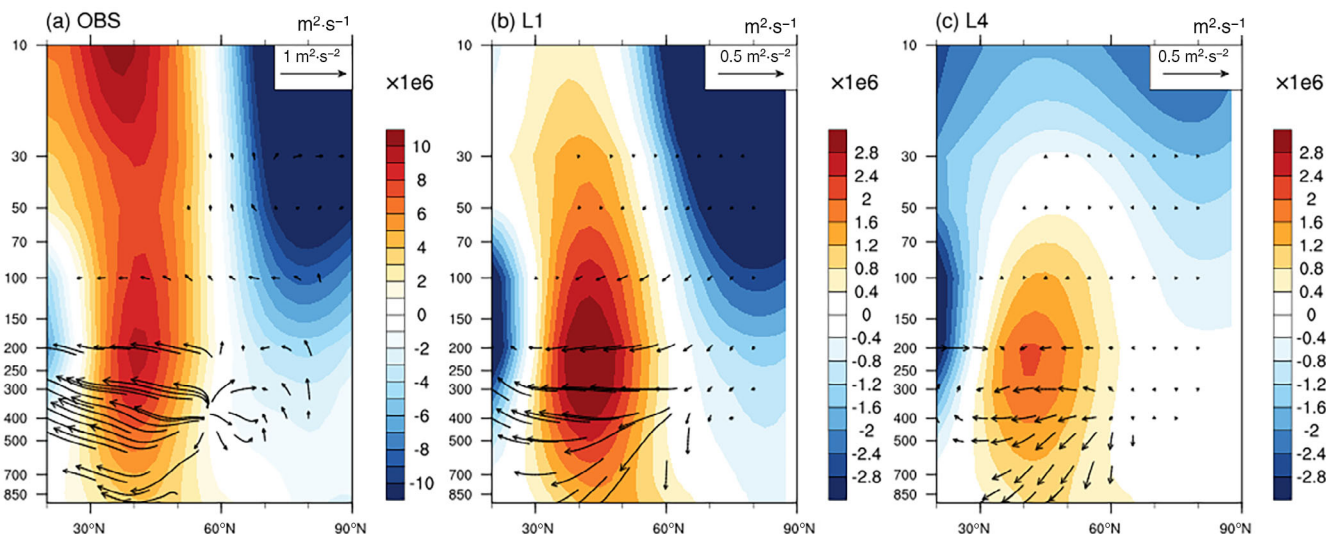


FIGURE 9 Vertical structure of composite difference of zonal mean WAF (vectors; m^2s^{-2}) and stream function (shading; m^2s^{-2}) over $160^\circ\text{--}120^\circ\text{W}$ between positive ($>0.5\sigma$) and negative ($<-0.5\sigma$) AO for (a) observation and MME for (b) 1-month and (c) 4-month lead during the period of DJF 1993/1994–2016/2017 [Colour figure can be viewed at wileyonlinelibrary.com]

defined as greater (less) than the 0.5 (-0.5) AO index standard deviations. In this observation, the stream function has a meridionally tripolar structure from the surface to the lower stratosphere, with a negative stream-function anomaly located over the tropics and Arctic and a positive stream function anomaly over the mid-latitudes. The vertical wave activity flux was superimposed over the stream function. The vertical wave activity flux indicates that the wave train originates from 60°N and spreads to the tropics and the Arctic. The wave activity flux was most active in the mid-latitudes, where the Aleutian Low was located. The pattern of the wave activity flux may be a factor contributing to AO and ENSO linkages at mid-latitudes. The MME for the 1-month lead represents the vertical tripolar structure of the stream function anomaly, but it fails to capture the maximum centre at 10 hPa over mid-latitudes. For the 4-month lead, the MME reversely shows the stream function anomaly 30 hPa above mid-latitude. The MME reproduces the pattern of the wave activity flux from 60°N to the tropics only in the troposphere, but the magnitude weakens during the 4-month lead. In addition, the MME for both the 1- and 4-month leads cannot present wave activity flux pattern from 60°N to the Arctic.

4 | DISCUSSION AND CONCLUSIONS

The purpose of this study is to understand the seasonal prediction skill of AO in terms of Z500 using 1- and 4-month lead MME. The MME consisted of five C3S

models and the PNU CGCM for the winter seasons for 1993/1994–2016/2017.

A large-scale seesaw pattern characterizes the AO, consisting of a negative Arctic Basin centre and two positive anomalous centres over the North Pacific and North Atlantic. The recent AO is slightly different from the pattern described in Thompson and Wallace (1998, 2000). The difference regards observations indicating North Pacific centre movement to the east. The ability of the MME to predict the AO index and represent the AO pattern for the same period generally decreases with the forecast lead time. Although some models perform better than the MME, the MME performs better than the arithmetic mean of single-model skills. In addition, the MME reproduces the zonally symmetric and barotropic vertical structures of geopotential height and zonal wind associated with AO relatively accurately, but the correlation decreases in the upper level, and its value decrease with forecast lead time.

In general, it is known that the AO is related to the EAWM (e.g., Gong *et al.*, 2001; Wu and Wang, 2002a; 2002b; Park *et al.*, 2010; Jeong *et al.*, 2017). In contrast, the weak AO–EAWM relationship and strong AO–ENSO connection are demonstrated during the DJF 1993/1994–2016/2017 in both the observation and MME, which are not consistent with previous studies (Gong *et al.*, 2001; Wu and Wang, 2002a; 2002b; Park *et al.*, 2010; Jeong *et al.*, 2017).

Li *et al.* (2014) reported that the AO–ENSO relationship has strengthened recently. Strong AO–ENSO relationships and weak AO–EAWM connections were found during DJF 1993/1994–2016/2017 in both observations

and the MME. The observations and the MME represent the active pattern of the wave activity flux from 60°N to the equator in the troposphere, so the wave activity flux may contribute to the connection between AO and ENSO in both observations and the MME. After the mid-1990s, significant in-phase correlation between the negative AO and Aleutian low (Li *et al.*, 2014) and the in-phase relationship between ENSO and the Aleutian low (Li *et al.*, 2014; Soulard *et al.*, 2019) may have contributed to the close relationship between AO and ENSO (Li *et al.*, 2014). The Aleutian low is strong in AO- and ENSO-related sea-level pressure, and the SH-related sea-level pressure is dissimilar to the AO impact. A strong Aleutian low was also found in the regressed field of the Z500, sea surface temperature, and 925 hPa wind. A strong AO–ENSO relationship was observed in both the observation and MME, and the AO–SH relationship appeared to persist in the MME prediction. This study is limited because of a short hindcast period; consequently, further study will be needed using a longer period to obtain more robust results.

ACKNOWLEDGEMENTS

The authors appreciate the institutes participating in the C3S seasonal forecast system for providing the hindcast experimental data. Gayoung Kim received support from the APEC Climate Center. Joong-Bae Ahn was supported by the Cooperative Research Program for Agriculture Science & Technology Development (Project No. PJ01489102), Rural Development Administration, Republic of Korea.

ORCID

Gayoung Kim  <https://orcid.org/0000-0001-6002-386X>

Joong-Bae Ahn  <https://orcid.org/0000-0001-6958-2801>

REFERENCES

- Chen, S., Chen, W. and Yu, B. (2018) Modulation of the relationship between spring AO and the subsequent winter ENSO by the preceding November AO. *Scientific Reports*, 8, 1–7. <https://doi.org/10.1038/s41598-018-25303-0>.
- Chen, S., Yu, B. and Chen, W. (2014) An analysis on the physical process of the influence of AO on ENSO. *Climate Dynamics*, 42, 973–989. <https://doi.org/10.1007/s00382-012-1654-z>.
- Chen, W., Hans-F, G. and Huang, R. (2000) The interannual variability of East Asian winter monsoon and its relation to the summer monsoon. *Advances in Atmospheric Sciences*, 17, 48–60. <https://doi.org/10.1007/s00376-000-0042-5>.
- Cohen, J., Zhang, X., Francis, J., Jung, T., Kwok, R., Overland, J., Ballinger, T.J., Bhatt, U.S., Chen, H.W., Coumou, D., Feldstein, S., Gu, H., Handorf, D., Henderson, G., Ionita, M., Kretschmer, M., Laliberte, F., Lee, S., Linderholm, H.W., Maslowski, W., Peings, Y., Pfeiffer, K., Rigor, I., Semmler, T., Stroeve, J., Taylor, P.C., Vavrus, S., Vihma, T., Wang, S., Wendisch, M., Wu, Y., and Yoon, J. (2020) Divergent consensuses on Arctic amplification influence on midlatitude severe winter weather. *Nature Climate Change*, 10, 20–29. <https://doi.org/10.1038/s41558-019-0662-y>.
- Dee, D.P., Medium, F., Weather, R., Fuentes, M., Medium, F., Weather, R., Kallberg, P. and Meteorological, S. (2009) *The ERA-Interim archive*. Reading: ECMWF.
- Dee, D.P., Uppala, S.M., Simmons, A.J., Berrisford, P., Poli, P., Kobayashi, S., Andrae, U., Balmaseda, M.A., Balsamo, G., Bauer, P., Bechtold, P., Beljaars, A.C.M., van de Berg, L., Bidlot, J., Bormann, N., Delsol, C., Dragani, R., Fuentes, M., Geer, A. J., Haimberger, L., Healy, S.B., Hersbach, H., Hólm, E.V., Isaksen, L., Kållberg, P., Köhler, M., Matricardi, M., McNally, A.P., Monge-Sanz, B.M., Morcrette, J.-J., Park, B.-K., Peubey, C., de Rosnay, P., Tavolato, C., Thépaut, J.-N. and Vitart, F. (2011) The ERA-Interim reanalysis: configuration and performance of the data assimilation system. *Quarterly Journal of the Royal Meteorological Society*, 137, 553–597. <https://doi.org/10.1002/qj.828>.
- Doblas-Reyes, F.J., Andreu-Burillo, I., Chikamoto, Y., García-Serrano, J., Guemas, V., Kimono, M., Mochizuki, T., Rodrigues, L.R.L., and van Oldenborgh, G.J. (2013) Initialized near-term regional climate change prediction. *Nature Communications*, 4, 1–9. <https://doi.org/10.1038/ncomms2704>.
- Gong, D.-Y. and Wang, S.-W. (2003) Influence of Arctic Oscillation on winter climate over China. *Journal of Geographical Sciences*, 13, 208–216.
- Gong, D.-Y., Wang, S.-W. and Zhu, J.-H. (2001) East Asian winter monsoon and Arctic Oscillation. *Geophysical Research Letters*, 28, 2073–2076. <https://doi.org/10.1029/2000GL012311>.
- Jeong, J.-H. and Ho, C.-H. (2005) Changes in occurrence of cold surges over East Asia in association with Arctic Oscillation. *Geophysical Research Letters*, 32, 1–4. <https://doi.org/10.1029/2005GL023024>.
- Jeong, J.-H., Lee, H., Yoo, J.H., Kwon, M.H., Yeh, S.W., Kug, J.S., Lee, J.Y., Kim, B.M., Son, S.W., Min, S.K., Lee, H., Lee, W.S., Yoon, J.H., and Kim, H.K. (2017) The status and prospect of seasonal climate prediction of climate over Korea and East Asia: a review. *Asia-Pacific Journal of Atmospheric Sciences*, 53, 149–173. <https://doi.org/10.1007/s13143-017-0008-5>.
- Jin, E.K., Kinter, J.L., Wang, B., Park, C.K., Kang, I.S., Kirtman, B. P., Kug, J.S., Kumar, A., Luo, J.J., Schemm, J., Shukla, J. and Yamagata, T. (2008) Current status of ENSO prediction skill in coupled ocean–atmosphere models. *Climate Dynamics*, 31, 647–664. <https://doi.org/10.1007/s00382-008-0397-3>.
- Kang, D., Lee, M.-I., Im, J., Kim, D., Kim, H.-M., Kang, H.-S., Schubert, S.D., Arribas, A., MacLachlan, C. (2014) Prediction of the Arctic Oscillation in boreal winter by dynamical seasonal forecasting systems. *Geophysical Research Letters*, 41, 3577–3585. <https://doi.org/10.1002/2014GL060011>.
- Kim, G., Ahn, J.-B., Kryjov, V.N., Lee, W.-S., Kim, D.-J. and Kumar, A. (2021) Assessment of MME methods for seasonal prediction using WMO LC-LRFMME hindcast dataset. *International Journal of Climatology*, 41, E2462–E2481. <https://doi.org/10.1002/joc.6858>.
- Kim, G., Ahn, J.-B., Kryjov, V.N., Sohn, S.-J., Yun, W.-T., Graham, R., Kolli, R.K., Kumar, A., and Ceron, J.-P. (2016) Global and regional skill of the seasonal predictions by WMO lead centre

- for long-range forecast multi-model ensemble. *International Journal of Climatology*, 36, 1657–1675. <https://doi.org/10.1002/joc.4449>.
- Kim, J., Yoon, D., Cha, D.H., Choi, Y., Joowan, K.I.M. and Son, S. W. (2019) Impacts of the East Asian winter monsoon and local sea surface temperature on heavy snowfall over the Yeongdong region. *Journal of Climate*, 32, 6783–6802. <https://doi.org/10.1175/JCLI-D-18-0411.1>.
- Kirtman, B.P., Min, D., Infanti, J.M., Kinter, J.L., Paolino, D.A., Zhang, Q., Van Den Dool, H., Saha, S., Mendez, M.P., Becker, E., Peng, P., Tripp, P., Huang, J., Dewitt, D.G., Tippett, M.K., Barnston, A.G., Li, S., Rosati, A., Schubert, S.D., Rienecker, M., Suarez, M., Li, Z.E., Marshak, J., Lim, Y.K., Tribbia, J., Pegion, K., Merryfield, W.J., Denis, B. and Wood, E.F. (2014) The North American multimodel ensemble: Phase-1 seasonal-to-interannual prediction; phase-2 toward developing intraseasonal prediction. *Bulletin of the American Meteorological Society*, 95, 585–601. <https://doi.org/10.1175/BAMS-D-12-00050.1>.
- Kryzhov, V.N. and Gorelits, O.V. (2015) The Arctic Oscillation and its impact on temperature and precipitation in northern Eurasia in the 20th century. *Russian Meteorology and Hydrology*, 40, 711–721. <https://doi.org/10.3103/S1068373915110011>.
- Lee, D.Y., Lin, W. and Petersen, M.R. (2020) Wintertime Arctic Oscillation and North Atlantic Oscillation and their impacts on the Northern Hemisphere climate in E3SM. *Climate Dynamics*, 55, 1105–1124. <https://doi.org/10.1007/s00382-020-05316-0>.
- Li, F., Wang, H. and Liu, J. (2014) The strengthening relationship between Arctic Oscillation and ENSO after the mid-1990s. *International Journal of Climatology*, 34, 2515–2521. <https://doi.org/10.1002/joc.3828>.
- Li, S., HE, S.P., Li, F. and WANG, H.J. (2018) Simulated and projected relationship between the East Asian winter monsoon and winter Arctic Oscillation in CMIP5 models. *Atmospheric and Oceanic Science Letters*, 11, 417–424. <https://doi.org/10.1080/16742834.2018.1512356>.
- Palmer, T.N., Doblus-Reyes, F.J., Hagedorn, R., Alessandri, A., Gualdi, S., Andersen, U., Feddersen, H., Cantelaube, P., Terres, J.-M., Davey, M., Graham, R., Délecluse, P., Lazar, A., Déqué, M., Guérémy, J.-F., Diez, E., Orfila, B., Hoshen, M., Morse, A. P., Keenlyside, N., Latif, M., Maisonnave, E., Rogel, P., Marletto, V. and Thomson, M.C. (2004) Development of a European multimodel ensemble system for seasonal-to-interannual prediction (Demeter). *Bulletin of the American Meteorological Society*, 85, 853–872. <https://doi.org/10.1175/BAMS-85-6-853>.
- Park, T.-W., Ho, C.-H., Yang, S. and Jeong, J.-H. (2010) Influences of Arctic Oscillation and Madden–Julian Oscillation on cold surges and heavy snowfalls over Korea: a case study for the winter of 2009–2010. *Journal of Geophysical Research*, 115, D23122. <https://doi.org/10.1029/2010JD014794>.
- Portal, A., Ruggieri, P., Palmeiro, F.M., García-Serrano, J., Domeisen, D.I.V. and Gualdi, S. (2021) Seasonal prediction of the boreal winter stratosphere. *Climate Dynamics*, 58, 2109–2130. <https://doi.org/10.1007/s00382-021-05787-9>.
- Reynolds, R.W., Smith, T.M., Liu, C., Chelton, D.B., Casey, K.S. and Schlax, M.G. (2007) Daily high-resolution-blended analyses for sea surface temperature. *Journal of Climate*, 20, 5473–5496. <https://doi.org/10.1175/2007JCLI1824.1>.
- Shin, S.-H. and Moon, J.-Y. (2018) Prediction skill for the East Asian winter monsoon based on APCC multi-models. *Atmosphere (Basel)*, 9, 1–18. <https://doi.org/10.3390/atmos9080300>.
- Soulard, N., Lin, H. and Yu, B. (2019) The changing relationship between ENSO and its extratropical response patterns. *Scientific Reports*, 9, 1–10. <https://doi.org/10.1038/s41598-019-42922-3>.
- Sun, J. and Ahn, J.-B. (2015) Dynamical seasonal predictability of the Arctic Oscillation using a CGCM. *International Journal of Climatology*, 35, 1342–1353. <https://doi.org/10.1002/joc.4060>.
- Takaya, K. and Nakamura, H. (2001) A formulation of a phase-independent wave-activity flux for stationary and migratory quasigeostrophic eddies on a zonally varying basic flow. *Journal of the Atmospheric Sciences*, 58, 608–627. [https://doi.org/10.1175/1520-0469\(2001\)058<0608:AFOAPI>2.0.CO;2](https://doi.org/10.1175/1520-0469(2001)058<0608:AFOAPI>2.0.CO;2).
- Thompson, D.W.J. and Wallace, J.M. (1998) The Arctic oscillation signature in the wintertime geopotential height and temperature fields. *Geophysical Research Letters*, 25, 1297–1300. <https://doi.org/10.1029/98GL00950>.
- Thompson, D.W.J. and Wallace, J.M. (2000) Annular mode in the extratropical circulation. Part I: month-to-month variability. *Journal of Climate*, 13, 1000–1016. [https://doi.org/10.1175/1520-0442\(2000\)013<1000:AMITEC>2.0.CO;2](https://doi.org/10.1175/1520-0442(2000)013<1000:AMITEC>2.0.CO;2).
- Wang, B., Lee, J.-Y., Kang, I.-S., Shukla, J., Park, C.-K., Kumar, A., Schemm, J., Cocke, S., Kug, J.-S., Luo, J.-J., Zhou, T., Wang, B., Fu, X., Yun, W.-T., Alves, O., Jin, E.K., Kinter, J., Kirtman, B., Krishnamurti, T., Lau, N.C., Lau, W., Liu, P., Pegion, P., Rosati, T., Schubert, S., Stern, W., Suarez, M. and Yamagata, T. (2009) Advance and prospectus of seasonal prediction: assessment of the APCC/ClipAS 14-model ensemble retrospective seasonal prediction (1980–2004). *Climate Dynamics*, 33, 93–117. <https://doi.org/10.1007/s00382-008-0460-0>.
- Wang, D., Wang, C., Yang, X. and Lu, J. (2005) Winter Northern Hemisphere surface air temperature variability associated with the Arctic Oscillation and North Atlantic Oscillation. *Geophysical Research Letters*, 32, 1–4. <https://doi.org/10.1029/2005GL022952>.
- Wang, H. and He, S. (2012) Weakening relationship between East Asian winter monsoon and ENSO after mid-1970s. *Chinese Science Bulletin*, 57, 3535–3540. <https://doi.org/10.1007/s11434-012-5285-x>.
- Wu, B. and Wang, J. (2002a) Winter Arctic Oscillation, Siberian High and East Asian winter monsoon. *Geophysical Research Letters*, 29, 3–6. <https://doi.org/10.1029/2002GL015373>.
- Wu, B. and Wang, J. (2002b) Possible impacts of winter Arctic Oscillation on Siberian High, the East Asian winter monsoon and sea-ice extent. *Advances in Atmospheric Sciences*, 19, 297–320. <https://doi.org/10.1007/s00376-002-0024-x>.
- Zuo, J.Q., Li, W.J. and Ren, H.L. (2013) Representation of the arctic oscillation in the CMIP5 models. *Advances in Climate Change Research*, 4, 242–249. <https://doi.org/10.3724/SP.J.1248.2013.242>.

SUPPORTING INFORMATION

Additional supporting information may be found in the online version of the article at the publisher's website.

How to cite this article: Kim, G., & Ahn, J.-B. (2022). Representation of the wintertime Arctic Oscillation in a multi-model ensemble. *International Journal of Climatology*, 1–12. <https://doi.org/10.1002/joc.7710>